

Turbulence-induced bubble nucleation in hydrothermal fluids beneath Yellowstone Lake

Corentin Caudron^{1,2}, Jean Vandemeulebrouck² & Robert A. Sohn³

Volcanic systems generate large amounts of gas, and understanding gas fluxes is a fundamental aspect of volcanology and hazard mitigation. Volcanic gases can be challenging to measure, but acoustic methods hold promise in underwater environments because gas bubbles are powerful sound sources. We deployed an acoustic system to study the nature of gas discharge at a large (~30 MW) thermal field on the floor of Yellowstone Lake, which has experienced numerous hydrothermal explosions since the last glaciation (~13.4 ka). We find that small (<10 Pa) turbulent flow instabilities trigger the nucleation of CO₂ bubbles in the saturated fluids. The observation of CO₂ bubbles nucleating in hydrothermal fluids due to small pressure perturbations informs our understanding of hydrothermal explosions in Yellowstone Lake, and demonstrates that acoustic data in underwater environments can provide insight into the stability of gas-rich systems, as well as gas fluxes.

¹Laboratoire G-Time, Department of Geosciences, Environment and Society, Université libre de Bruxelles, Brussels, Belgium. ²ISTerre, Université Grenoble Alpes, Université Savoie Mont Blanc, CNRS, IRD, IFSTTAR, 38000 Grenoble, France. ³Woods Hole Oceanographic Institution, Woods Hole, MA, USA.
email: corentin.caudron@ulb.be

Gas fluxes through volcanic systems constitute an important component of the global cycle for elements such as carbon¹ and sulfur², and they present a significant geological hazard for communities located near volcanic systems^{3,4}. Gas species can be difficult to accurately measure in subaerial environments due to the intrinsic difficulties associated with sampling, and the relatively high atmospheric concentrations of dominant species such as CO₂^{5,6}. Most volcanic systems, however, are located underwater⁷, and many others host intracaldera lakes, which opens the possibility of using acoustic methods to monitor gas fluxes. Gas bubbles are energetic sound sources, and recent studies have demonstrated that acoustic methods can effectively detect gas fluxes in volcanic lakes^{8,9}, in much the same way they are being used to monitor gas fluxes during CO₂ storage experiments¹⁰ and in CH₄ seep environments¹¹.

The Yellowstone Plateau Volcanic Field (YPVF) constitutes one of the largest volcanic systems on Earth, and although it has not experienced a volcanic eruption for the past ~70 ky¹², it is presently discharging magmatic CO₂ at an estimated rate of ~32 kt day⁻¹¹³. This flux estimate, however, is uncertain by a factor of ~3 due to inaccuracies in gas accumulation chamber measurements¹³, and it does not include any fluxes into Yellowstone's hydrothermally active lakes. Yellowstone Lake, which straddles the southeast margin of the 640 ka Yellowstone Caldera, is the largest lake in the YPVF and it hosts a variety of hydrothermal fields, including both liquid- and vapor-dominated systems at depths of up to ~110 m below the lake surface¹⁴. The hydrothermal systems beneath Yellowstone Lake have generated more than a dozen large explosions over the past ~13,000 years, including the Mary Bay explosion (13,400 years ago), which created a ~2.6 km wide by ~115 m deep crater on the lake floor, and distributed debris over an area of ~30 km²¹⁵. The gas fluxes from these sublacustrine systems are largely unknown, but a recent multidisciplinary study¹⁶ has shown that the “Deep Hole” thermal field, located to the southeast of Stevenson Island (Fig. 1a), is among the most energetic (~30 MW) thermal areas on the YPVF¹⁷. Fluids discharging from the Deep Hole are hot (mean temperature of 49 measured vents = 132 °C, with a range of 74–174 °C¹⁸) and rich in CO₂ and H₂S dissolved gases¹⁹. The vents are located within a set of superimposed pockmarks that may have been generated by sediment expulsion associated with the episodic release of gas²⁰. The role of magmatic gases in these explosions is unclear, but the release of trapped gas from a subsurface reservoir and the exsolution of dissolved gases from

hydrothermal fluids are poorly understood, but potentially explosive, processes²¹.

We used acoustic methods to monitor gas fluxes at the Deep Hole thermal field for 13 h when ambient noise levels in the lake were low (overnight). We detected a 3-h interval of intense activity, during which small pressure fluctuations at frequencies of ~1–40 Hz, interpreted to be turbulent flow instabilities in discharging fluids, triggered the nucleation of CO₂ bubbles near the lake floor interface. Bubble nucleation at relatively small amplitudes (~tens of Pa) requires the presence of pre-existing microbubbles in the hydrothermal fluids, and indicates that the subsurface fluids could be unstable to larger pressure fluctuations, such as might be associated with earthquakes, for example.

Results and discussion

We deployed an audio-quality (44.1 kHz, 24 bit) acoustic hydrophone (Supplementary Fig. 1) in the Deep Hole thermal field (Fig. 1) at a depth of ~115 m on the floor of Yellowstone Lake to investigate the effectiveness of acoustic measurements for monitoring gas fluxes in this environment. The system was deployed in an area of active, but relatively weak discharge, ~100 m north of the main vent field, where conductive heat flow through the sediments is roughly half (~25 W m⁻²) that measured in the main field. We recorded 13 h of continuous data, within which we observed a 3-h interval (23:40 16 August to 02:30 17 August, UTC) of intense activity. Sixty-six discrete events were detected during this interval (see “Methods”), all exhibiting a characteristic waveform (Fig. 2) consisting of a brief (~1 ms), high-frequency (several kHz; Fig. 2 and Supplementary Fig. 2), impulsive onset, followed by lower frequency (~100–200 Hz) oscillations. The event durations scale with amplitude, with the largest amplitude signals having durations of up to 50 ms, but typical durations of ~10 ms (Fig. 2). The intense rate of activity (~0.5 event/min) suddenly stops at ~2.30, and no additional events were detected until the end of the recording (13:00 17 August).

The acoustic signals are consistent with bubble nucleation events (hereafter referred to as “bubble events”), where the impulsive, high-frequency onset is generated by opening of a void space in the liquid, and the subsequent, lower-frequency signal is generated by free oscillations of the newly formed bubble^{22,23}. The acoustic data do not directly constrain the composition of the bubbles, which could either be vapor or a non-condensable gas. Videographic data from remotely operated vehicle (ROV) dives demonstrate that bubble discharge is ubiquitous from active vents

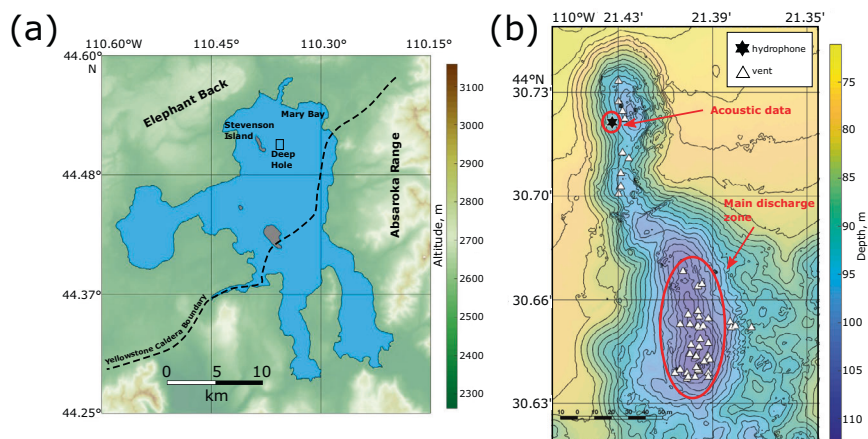


Fig. 1 Location. **a** Yellowstone Lake (USA). The northern part of the lake lies inside the 640 ka Yellowstone Caldera (dashed line). **b** Bathymetry of the Deep Hole thermal area (black rectangle in left panel). White triangles indicate active venting locations observed during remotely operated vehicle dives, and the black star corresponds to the hydrophone location. The spatial extent of the main discharge zone is shown with a red ellipse.

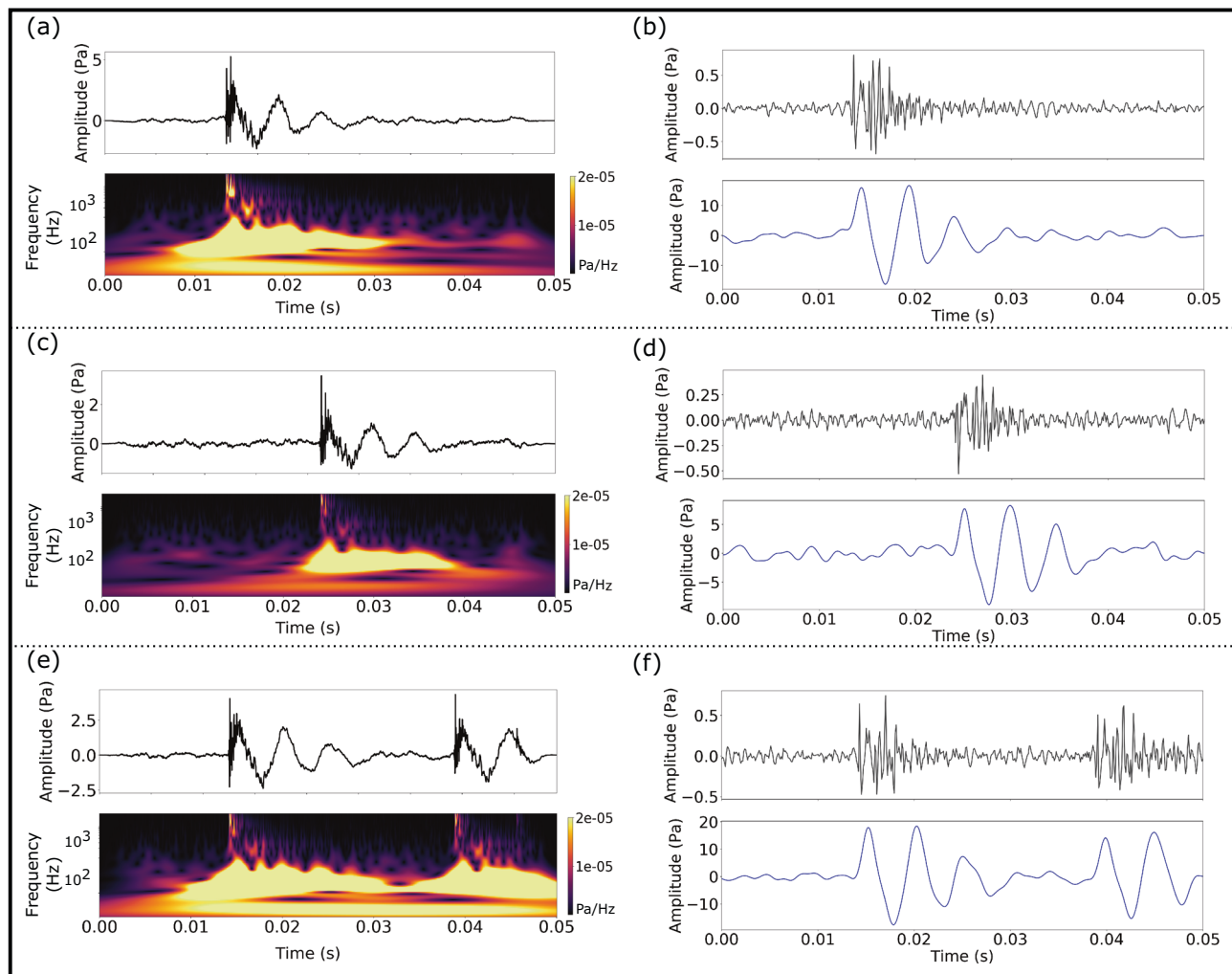


Fig. 2 Time-frequency characteristics of bubble events. **a, c, e** Typical waveform and corresponding time-frequency evolution (wavelet transform) of four bubbles (**e** contains two events). **b, d, f** Filtering to isolate the impulsive and resonant components of the waveforms. Top panel (black) shows the impulsive onset (high-pass filtered above 600 Hz), and bottom panel (blue) shows the resonance of ~100–200 Hz (low-pass filtered below 600 Hz).

in the Deep Hole, with diameters in the mm–cm range, and that these bubbles do not condense upon discharge into the lake, but rather rise significant distances through the water column, with some rising all the way to the lake surface. Assuming that the bubbles we detected acoustically have the same composition as the bubbles observed during ROV dives, the fact that the bubbles do not condense upon encountering $\sim 4^\circ\text{C}$ lake water indicates that they are not dominantly composed of vapor, but rather must be a non-condensable gas. This conclusion is supported by temperature measurements in fluid upflow zones near our observation site, which are well below saturation values¹⁹. Chemical analyses of Deep Hole fluids acquired with gas-tight samplers indicate CO_2 saturation^{20,24} leading to the conclusion that the bubbles are dominantly composed of CO_2 . Applying Minnaert’s equation for the relationship between oscillation frequency and the radius of a spherical bubble²² of CO_2 (see “Methods”) yields radii ranging from 1.6–3.6 cm, with a median bubble volume of 3.34×10^{-5} L (Supplementary Fig. 3). These size estimates are compatible with, though on the large side of, bubbles observed during ROV dives (Supplementary Video 1).

Visual inspection of the records reveals that most (>70%) of the bubble events are immediately preceded (<1 s) by short (~ 400 ms) pressure pulses at frequencies below ~ 40 Hz (Fig. 3). These signals occur more frequently (5/min) than the bubble events

(0.4/min), but a statistical analysis confirms that there is a non-random association between the event times, with bubble events preferentially occurring after a low-frequency event (see “Methods”). A typical pulse begins with a rise to a pressure maximum (compression), followed by a drop to a pressure minimum (decompression), and the bubble events preferentially occur when the decompression rate is maximal (~ 50 Pa/s for non-normalized amplitudes) during the initial pressure drop (Fig. 3), consistent with hydrodynamic cavitation in a flowing fluid²⁵ (i.e., bubble nucleation when the dynamic pressure reaches a threshold value²⁶). Of all the potential mechanisms by which hydrothermal fluid flow may generate noise²⁷, unsteady turbulence or flow noise²⁸ provide the most likely explanations for the low-frequency pulses we observed. The Reynolds number of the hot hydrothermal fluids being discharged at the Deep Hole field is on the order of $\sim 1 \times 10^5$, which is in the turbulent flow regime¹⁸, and turbulent interaction of the fluids with conduits in the sediments could produce acoustic energy in the 1–40 Hz band.

We thus interpret the acoustic signals we observed as stochastic triggering of CO_2 bubble nucleation in the saturated hydrothermal fluids due to turbulent flow instabilities near the lake floor interface (Fig. 4). For fluids with the CO_2 concentrations measured for the Deep Hole (i.e., supersaturation values $< \sim 10$), this process can only occur if there are pre-existing gas cavities in

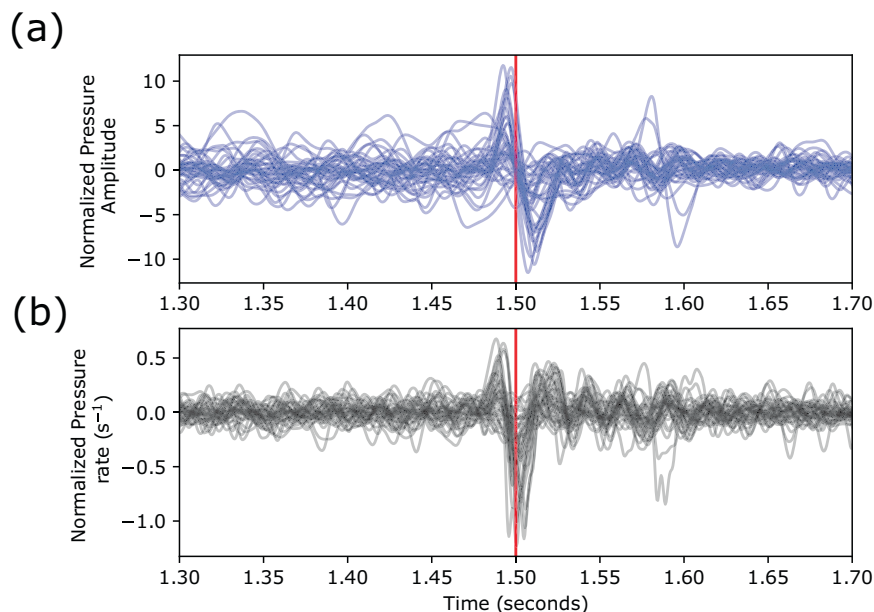


Fig. 3 Timing of bubble events relative to low-frequency pressure fluctuations. A subset of the low-frequency (filtered between 2 and 40 Hz) pressure signals (**a**, blue), and the corresponding pressure rate (**b**, black), aligned by time of bubble nucleation (red lines), showing that bubble nucleation preferentially occurs at the time of maximum decompression rate. The amplitudes have been normalized by removing the mean and dividing by the standard deviation.

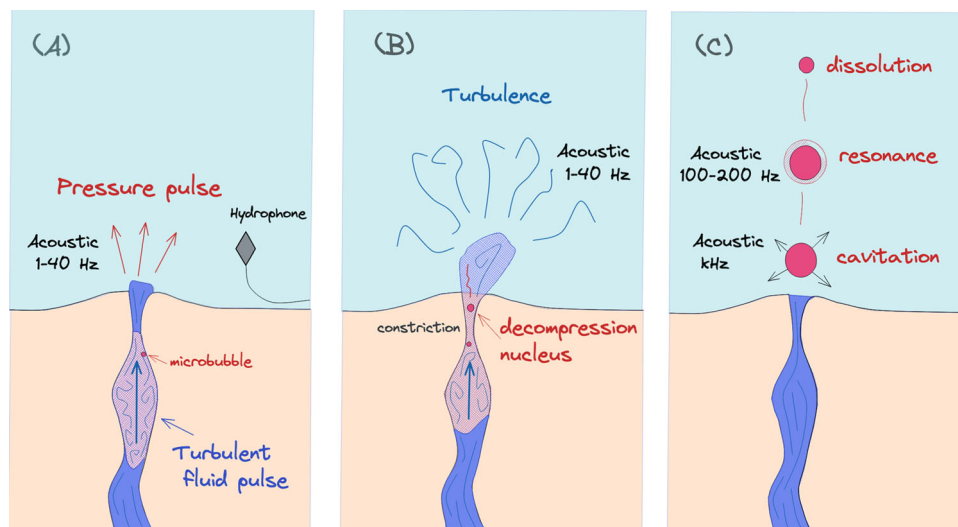


Fig. 4 Conceptual model. **A** A flow instability generated by the interaction of the hydrothermal fluid with the sediment matrix (e.g., a flowpath constriction), momentarily depressurizes the fluid, triggering the nucleation of a CO₂ bubble in the saturated fluid with pre-existing microbubbles (**B**). The bubble oscillates at its natural frequency before dissolving into the under-saturated lake water or rising to the lake surface (**C**).

the fluid²⁹. These metastable gas cavities could be located on the rough surfaces of the conduit walls or in the bulk solution, but without them the energy barrier for nucleation is too large to be overcome by the relatively small pressure fluctuations we measured. The constrictions triggering unsteady flow could be generated by mineral precipitation and alteration associated with hydrothermal flow²⁴, which can rapidly change the shape of the flow conduits³⁰, and which could also trap microbubbles.

The gas flux associated with the CO₂ bubbles in our records is $\sim 4.98 \times 10^{-6}$ kg/s, which is very small compared to the dissolved CO₂ flux through the Deep Hole thermal area. The main discharge zone contained at least 20 active vents (Fig. 1b) and had an estimated total fluid discharge rate of ~ 56 kg/s at the time of our measurements¹⁸. These fluids have a CO₂ concentration of

$\sim 7\text{--}18$ mmol/kg¹⁴, yielding a dissolved CO₂ flux through the main discharge zone of $\sim 46\text{--}119$ kg/s. Vents in the main zone discharge gas bubbles, but the offset distance is too great to detect them in our records³¹, such that we cannot use our data to constrain bubble fluxes for the Deep Hole thermal field, as a whole. Nevertheless, it seems clear that the gas flux through bubbles is likely a small fraction of the dissolved flux.

The nucleation of non-condensable gas bubbles due to unsteady flow informs our understanding of the stability of the lake floor hydrothermal systems, and their potential to generate explosions. Yellowstone Lake has experienced numerous hydrothermal explosions since the last glaciation in the area¹⁵. Two distinct categories of explosions have been identified: “large” explosions likely triggered by vaporization of hot, subsurface

liquids, and “small” explosions likely triggered by the episodic release and simple expansion of gas. Our results are relevant to the triggering of small explosions, which may be responsible for the pockmarks that cover the lake floor in hydrothermal areas, including the Deep Hole where our data were acquired. The bubble events we observed were triggered by instabilities with typical amplitudes of 10^{-1} –10 Pa (or 100–140 dB ref. 1 μ Pa) and maximum decompression rates of \sim 50 Pa/s measured at the hydrophone. We do not know the precise location of the bubble sources relative to the hydrophone, but the offset distance was likely no more than \sim 5 m considering the transmission loss at 350 Hz³², yielding instability amplitudes of \sim 10 to 250 Pa in the source region.

Nucleation of CO₂ bubbles due to these small, flow-induced, pressure fluctuations, suggests that larger pressure drops, such as might be associated with an earthquake, for example, could trigger larger-scale nucleation of CO₂ bubbles in subsurface fluids and generate a small hydrothermal explosion. Hydrothermal fluids sampled from the Deep Hole are saturated in CO₂, and the vents, themselves, discharge quasi-steady streams of non-condensable gas bubbles. The lid of the gas reservoir feeding the vents is at a depth of no more than \sim 15 m below the lake floor^{18,19}. The sediments beneath the Deep Hole are thus a gas-rich environment, and our results indicate that exsolution of dissolved gases can be triggered by small, but fast, pressure perturbations. This process is only possible at the CO₂ concentrations observed for the Deep Hole fluids if there are metastable microbubbles in the fluids that serve as nuclei for bubble growth. The microbubbles destabilize the fluid response to pressure drops, and, more generally, the high CO₂ concentrations in the subsurface fluids enhances their explosivity³³.

Our data from Yellowstone Lake further demonstrate the utility of acoustic methods for studying gas fluxes in underwater environments, and provide new insight into the nucleation of non-condensable gas bubbles in hydrothermal fluids. If hydrothermal fluids are saturated with non-condensable gases, they can be susceptible to expansion in response to pressure fluctuations, and this may explain the presence of pockmark fields and large sinkholes that have been observed at other caldera^{34–36} and crater-hosted lakes³⁷. Considering that more than 75% of Earth’s volcanism occurs underwater⁷, our results support the idea that acoustic methods have the potential to play an important role in monitoring and measuring volcanic gas fluxes⁸ at the global scale, which is one of the centennial grand challenges highlighted by the scientific community³⁸.

Methods

The hydrophone sensor was a High Tech HTI-90-U hydrophone (Supplementary Fig. 1), with a nominal frequency response of 2 Hz to 20 kHz. The instrument location is shown on Fig. 1b (\sim 30 cm above the lake floor). The acoustic records were first visually inspected before choosing the short term average/long term average (STA/LTA) parameters (STA of 0.3 s, LTA of 5 s) for event detection. Each detection event was verified manually to remove any spurious detections from the final catalogs. To characterize the signals, we first resampled them to 2000 Hz because the characteristic signals have dominant frequencies around 200 Hz. For the low-frequency signals, we low-pass filtered the signals below 50 Hz before computing the STA/LTA. We then automatically calculated the dominant frequencies for the 66 bubble signals using both wavelet (Morlet³⁹) and Fourier⁴⁰ transforms (Supplementary Fig. 4). We removed the mean and the linear trend, and tapered the signal with a Hanning window (10%) before conducting spectral analyses. The data processing was done using Obspy⁴¹.

Based on the dominant frequency, we compute the radius (r) using Minnaert’s²² relation, assuming an adiabatic equation of state for the gas in the bubble:

$$r = \frac{(3P\gamma/\rho)^{1/2}}{2\pi f}$$

Where P is the hydrostatic pressure (1079 kPa), γ is the ratio of specific heats of the gas in the bubble (1.3 for CO₂), ρ is the density of the liquid (1000 kg/m³) and f is the dominant frequency (in Hz).

We calculate the volume for each bubble, assuming they are all spherical ($V = 4/3\pi r^3$), then compute the cumulative volume. We then multiply by the density of CO₂ at these pressures (13.31 kg/m³) and divide by total time of bubble records (i.e., 3 h). We estimate the flux to 4.98×10^{-6} kg/s.

Uniformity plots (Supplementary Fig. 5) demonstrate that the bubble events can be modeled as a Poisson process, where the event times are uniformly distributed over the observation interval. Assuming a Poisson process, we used a parametric bootstrap test to assess the association between the bubble events (66) and the low-frequency events (665), with the test statistic equal to the mean delay time between each bubble event and the immediately preceding low-frequency event. To implement the test, we generated 1000 bootstrap replicates of the bubble event catalog sampled using a uniform distribution, and calculated the mean delay time for each replicate catalog, keeping the low-frequency event times fixed. Only two of these replicate catalogs had mean delays times less than the observed value, yielding a p value of 0.002, with an approximate error of \pm 0.001. This test demonstrates that the bubble events are associated with a preceding low-frequency event to a very high degree of confidence.

Data availability

The datasets generated during and/or analyzed during the current study are available from the corresponding author. The data that support the findings of this study are archived and are available from the Marine Geophysical Data Center (<https://www.marine-geo.org/tools/files/30446>).

Code availability

We analyzed the data using existing functions/routines from python packages (Matplotlib⁴², Obspy^{41,43} and Librosa⁴⁴). No function has been developed but any script is available from the corresponding author.

Received: 25 August 2021; Accepted: 17 March 2022;

Published online: 29 April 2022

References

- Plank, T. & Manning, C. E. Subducting carbon. *Nature* **574**, 343–352 (2019).
- Carn, S. A., Clarisse, L. & Prata, A. J. Multi-decadal satellite measurements of global volcanic degassing. *J. Volcanol. Geotherm. Res.* **311**, 99–134 (2016).
- Le Guern, F., Tazieff, H. & Pierret, R. F. An example of health hazard: people killed by gas during a phreatic eruption: Dieng plateau (Java, Indonesia), February 20th 1979. *Bull. Volcanol.* **45**, 153–156 (1982).
- Kling, G. W. et al. The 1986 Lake Nyos Gas Disaster in Cameroon, West Africa. *Science* **236**, 169–175 (1987).
- Schwandner, F. M. et al. Spaceborne detection of localized carbon dioxide sources. *Science* **358**, eaam5782 (2017).
- Aiuppa, A., Fischer, T. P., Plank, T. & Bani, P. CO₂ flux emissions from the Earth’s most actively degassing volcanoes, 2005–2015. *Sci. Rep.* **9**, 1–17 (2019).
- Dziak, R. P. et al. Long-term explosive degassing and debris flow activity at West Mata submarine volcano. *Geophys. Res. Lett.* **42**, 1480–1487 (2015).
- Vandemeulebrouck, J. et al. Hydroacoustic noise precursors of the 1990 eruption of Kelut Volcano, Indonesia. *J. Volcanol. Geotherm. Res.* **97**, 443–456 (2000).
- Caudron, C., Mazot, A. & Bernard, A. Carbon dioxide dynamics in Kelud volcanic lake. *J. Geophys. Res. Solid Earth* **117**, B05102 (2012).
- Blackford, J. et al. Detection and impacts of leakage from sub-seafloor deep geological carbon dioxide storage. *Nat. Clim. Change* **4**, 1011–1016 (2014).
- Veloso, M., Greinert, J., Mienert, J. & Batist, M. D. A new methodology for quantifying bubble flow rates in deep water using splitbeam echosounders: Examples from the Arctic offshore NW-Svalbard. *Limnol. Oceanogr. Methods* **13**, 267–287 (2015).
- Christiansen, R. L. *The Quaternary and Pliocene Yellowstone Plateau Volcanic Field of Wyoming, Idaho, and Montana*. (U.S. Department of the Interior, U.S. Geological Survey, 2001).
- Hurwitz, S. & Lowenstern, J. B. Dynamics of the Yellowstone hydrothermal system. *Rev. Geophys.* **52**, 375–411 (2014).
- Fowler, A. P. G. et al. Geochemical heterogeneity of sublacustrine hydrothermal vents in Yellowstone Lake, Wyoming. *J. Volcanol. Geotherm. Res.* **386**, 106677 (2019).
- Morgan, L. A., Shanks, W. C. & Pierce, K. L. *Hydrothermal Processes Above the Yellowstone Magma Chamber: Large Hydrothermal Systems and Large Hydrothermal Explosions*. 459 (Geological Society of America, 2009).
- Sohn, R. et al. Exploring the restless floor of Yellowstone Lake. *Eos* (2017).
- Sohn, R. A. et al. Observations and modeling of a hydrothermal plume in Yellowstone Lake. *Geophys. Res. Lett.* **46**, 6435–6442 (2019).

18. Favorito, J. E., Harris, R. N., Sohn, R. A., Hurwitz, S. & Luttrell, K. M. Heat flux from a vapor-dominated hydrothermal field beneath Yellowstone Lake. *J. Geophys. Res. Solid Earth* **126**, e2020JB021098 (2021).
19. Fowler, A. P. G. et al. Vapor-driven sublacustrine vents in Yellowstone Lake, Wyoming, USA. *Geology* **47**, 223–226 (2019).
20. Morgan, L. A. et al. Exploration and discovery in Yellowstone Lake: results from high-resolution sonar imaging, seismic reflection profiling, and submersible studies. *J. Volcanol. Geotherm. Res.* **122**, 221–242 (2003).
21. Thiéry, R. & Mercury, L. Explosive properties of water in volcanic and hydrothermal systems. *J. Geophys. Res. Solid Earth* **114**, B05205 (2009).
22. Minnaert Sc.D., M. XVI. On musical air-bubbles and the sounds of running water. *Lond. Edinb. Dublin Philos. Mag. J. Sci.* **16**, 235–248 (1933).
23. Mellen, R. H. Ultrasonic spectrum of cavitation noise in water. *J. Acoust. Soc. Am.* **26**, 356–360 (1954).
24. Shanks, W., Alt, J. & Morgan, L. Geochemistry of sublacustrine hydrothermal deposits in Yellowstone Lake—Hydrothermal Reactions, Stable-Isotope Systematics, Sinter Deposition, and Spire Formation. (U.S. Geological Survey, 2007).
25. Chang, N. A. & Ceccio, S. L. The acoustic emissions of cavitation bubbles in stretched vortices. *J. Acoust. Soc. Am.* **130**, 3209–3219 (2011).
26. Brennen, C. E. *Cavitation and Bubble Dynamics* (Cambridge University Press, 2014).
27. Crone, T. J., Wilcock, W. S. D., Barclay, A. H. & Parsons, J. D. The sound generated by mid-Ocean Ridge Black smoker hydrothermal vents. *PLoS ONE* **1**, e133 (2006).
28. Bassett, C., Thomson, J., Dahl, P. H. & Polagye, B. Flow-noise and turbulence in two tidal channels. *J. Acoust. Soc. Am.* **135**, 1764–1774 (2014).
29. Jones, S. F., Evans, G. M. & Galvin, K. P. Bubble nucleation from gas cavities—a review. *Adv. Colloid Interface Sci.* **80**, 27–50 (1999).
30. Kennedy, B. M. et al. Pressure controlled permeability in a conduit filled with fractured hydrothermal Breccia reconstructed from Ballistics from Whakaari (White Island), New Zealand. *Geosciences* **10**, 138 (2020).
31. Leighton, T. G. & White, P. R. Quantification of undersea gas leaks from carbon capture and storage facilities, from pipelines and from methane seeps, by their acoustic emissions. *Proc. R. Soc. Math. Phys. Eng. Sci.* **468**, 485–510 (2012).
32. Li, J. et al. Passive acoustic monitoring of a natural CO₂ seep site—implications for carbon capture and storage. *Int. J. Greenh. Gas Control* **93**, 102899 (2020).
33. Hurwitz, S. et al. Dissolved gases in hydrothermal (phreatic) and geyser eruptions at Yellowstone National Park, USA. *Geology* **44**, 235–238 (2016).
34. Pearson, L. K. *The Nature, Composition and Distribution of Sediment in Lake Rotorua, New Zealand* (The University of Waikato, 2007).
35. Anzidei, M. et al. The Albano Maar Lake high resolution bathymetry and dissolved CO₂ budget (Colli Albani volcano, Italy): constrains to hazard evaluation. *J. Volcanol. Geotherm. Res.* **171**, 258–268 (2008).
36. Andrade, C., Viveiros, F., Cruz, J. V. & Coutinho, R. Global carbon dioxide output of volcanic lakes in the Azores archipelago, Portugal. *J. Geochem. Explor.* **229**, 106835 (2021).
37. de Ronde, C. E. J. et al. Reconstruction of the geology and structure of Lake Rotomahana and its hydrothermal systems from high-resolution multibeam mapping and seismic surveys: effects of the 1886 Tarawera Rift eruption. *J. Volcanol. Geotherm. Res.* **314**, 57–83 (2016).
38. Fischer, T. P. & Aiuppa, A. AGU Centennial Grand Challenge: volcanoes and deep carbon global CO₂ emissions from subaerial volcanism—recent progress and future challenges. *Geochem. Geophys. Geosystems* **21**, e2019GC008690 (2020).
39. Kristeková, M., Kristek, J., Moczo, P. & Day, S. M. Misfit criteria for quantitative comparison of seismograms. *Bull. Seismol. Soc. Am.* **96**, 1836–1850 (2006).
40. Cooley, J. W. & Tukey, J. W. An algorithm for the machine calculation of complex Fourier series. *Math. Comput.* **19**, 297–301 (1965).
41. Krischer, L. et al. ObsPy: a bridge for seismology into the scientific Python ecosystem. *Comput. Sci. Discov* **8**, 014003 (2015).
42. Hunter, J. D. Matplotlib: a 2D graphics environment. *Comput. Sci. Eng.* **9**, 90–95 (2007).
43. Beyreuther, M. et al. ObsPy: a python toolbox for seismology. *Seismol. Res. Lett.* **81**, 530–533 (2010).
44. McFee, B. et al. librosa: audio and music signal analysis in Python. 18–24. <https://doi.org/10.25080/Majora-7b98e3ed-003> (2015).

Acknowledgements

The authors thank Alan Gardner for development of the hydrophone and audio recording package, Andy Solow for helpful statistical advice, and The Global Foundation for Ocean Exploration for logistical support during field work. We thank the Yellowstone National Park Resources office for the support required to conduct research within Yellowstone National Park. This research was supported by the National Science Foundation grant EAR-1516361 to R.A.S. All work in Yellowstone National Park was completed under an authorized research permit (YELL-2018-SCI-7018). We also acknowledge the IRGA 2021 Volcan project (funded by Université Grenoble Alpes) and Thomas Jefferson Fund Face Foundation (project TJJF20_009 ‘Quantifying underwater volcano degassing using novel seismo-acoustic approaches’). This paper benefited from various python packages including Matplotlib⁴², Obspy^{41,43} and Librosa⁴⁴. We also would like to thank the editor and the reviewer Christian Montanaro, as well as two anonymous reviewers, for their insightful suggestions and remarks.

Author contributions

R.A.S. acquired the data. J.V. and C.C. analyzed the recordings. All the authors contributed to the interpretation and writing.

Competing interests

The authors declare no competing interests.

Additional information

Supplementary information The online version contains supplementary material available at <https://doi.org/10.1038/s43247-022-00417-6>.

Correspondence and requests for materials should be addressed to Corentin Caudron.

Peer review information *Communications Earth & Environment* thanks Cristian Montanaro and the other, anonymous, reviewer(s) for their contribution to the peer review of this work. Primary Handling Editors: Emma Liu, Joe Aslin and Clare Davis. Peer reviewer reports are available.

Reprints and permission information is available at <http://www.nature.com/reprints>

Publisher's note Springer Nature remains neutral with regard to jurisdictional claims in published maps and institutional affiliations.



Open Access This article is licensed under a Creative Commons Attribution 4.0 International License, which permits use, sharing, adaptation, distribution and reproduction in any medium or format, as long as you give appropriate credit to the original author(s) and the source, provide a link to the Creative Commons license, and indicate if changes were made. The images or other third party material in this article are included in the article's Creative Commons license, unless indicated otherwise in a credit line to the material. If material is not included in the article's Creative Commons license and your intended use is not permitted by statutory regulation or exceeds the permitted use, you will need to obtain permission directly from the copyright holder. To view a copy of this license, visit <http://creativecommons.org/licenses/by/4.0/>.

© The Author(s) 2022